Journal of Membrane Science 399–400 (2012) 73–85

Contents lists available at SciVerse ScienceDirect

Journal of Membrane Science

journal homepage: www.elsevier.com/locate/memsci

Multilayer reactive barrier materials

S. Carranza, D.R. Paul, R.T. Bonnecaze *

Department of Chemical Engineering, The University of Texas at Austin, 1 University Station CO400, Austin, TX 78712, United States

ARTICLE INFO

Article history:
Received 25 October 2011
Received in revised form 21 January 2012
Accepted 24 January 2012
Available online 2 February 2012

Keywords:
Reactive membranes
Multilayer
Packaging
Oxygen scavenging

ABSTRACT

A model is developed and solved analytically and numerically to describe the barrier properties of multilayer films with alternating reactive and inert layers. Incorporation of reactive scavenging sites in packaging materials can significantly improve their barrier properties. Due to mechanical and optical requirements, barrier films typically consist of polymer blends or multilayer films of the scavenging material and an inert supporting polymer. Because composite reactive barriers are expected to operate for months or years, purely experimental characterization is not practical and models are needed to optimize the configurations and to confidently extrapolate experimental data. The model for multilayer films is solved numerically over a wide parameter space, varying physical properties and layer configuration to determine the flux and time lag. Asymptotic analysis of the model is used to develop analytical predictions for transport behavior at early and long times. The performance of multilayer composites is compared to polymer blends and discussion of the most suitable configuration for different scenarios is presented.

1. Introduction

Composites containing reactive polymers can be used to significantly improve the barrier performance of packaging materials (e.g.; [1–3] and references within). For example, polymers that readily oxidize, such as polybutadiene [4–8], may be used to scavenge oxygen, temporarily reducing oxygen permeation until the scavenger has been exhausted. Two common reactive barrier configurations are polymer blends and multilayer films. Analytical equations to predict barrier transport have been developed for polymer blends [3].

Here we develop a model and analytic equations for the transport in barriers formed by alternating layers of an inert polymer, such as polyethylene terephthalate (PET), and a reactive/scavenging polymer, such as polybutadiene. This is motivated by microlayer coextrusion technology that enables the fabrication of films with a large number of layers [9,10]. The models and results presented here are developed in the context of oxygen scavenging, but they are generally applicable to any reactive permeate and barrier system.

The time lag, which is about the time it takes for a steady-state concentration profile to be established across a scavenging barrier film (or more precisely the time when the asymptotic cumulative flux intercepts the time axis, e.g. Fig. 5b), indicates the exhaustion of reactive sites and has been traditionally used as the figure of merit for reactive barriers. While time lag is an important figure of merit, with analytical expressions available for homogeneous films [11] and polymer blends [1], it does not predict how much solute (e.g., oxygen or water) will permeate up to that point. Recently, an initial flux plateau has been identified as a measure of the leakage flux at early times [2,3].

Previous modeling efforts for layered films [12–15] focused on the best placement of a single reactive layer within a film of one or more inert layers. Nuxoll et al. [12] developed a prediction for time lag for a layered barrier where a single reactive layer could be placed at different locations within an inert matrix. However, an understanding of the effect of number and ordering of layers on barrier performance for multilayer films is lacking.

The purpose of this paper is to develop models and design equations to predict the barrier performance of multilayer films and to define the ranges of validity of the predictive equations. The models and equations are used to predict the effect of layer configuration (i.e., number and sequence of layers) and of physical properties (i.e., diffusion and solubility coefficients of reactive and inert layers, the reaction rate constant, etc.) on performance. Finally, the performance of multilayer films is compared to that of polymer blends, enabling the selection of the most suitable configuration for a particular set of requirements.

2. Model description

Consider a film of thickness L consisting of N_M inert matrix layers and N_R reactive (scavenging) layers arranged in an alternating pattern, with a total of $N = N_M + N_R$ layers, as illustrated in Fig. 1.

* Corresponding author. Tel.: +1 512 471 1497; fax: +1 512 471 7060.
E-mail address: rtb@che.utexas.edu (R.T. Bonnecaze).

0376-7388/$ – see front matter © 2012 Elsevier B.V. All rights reserved.
doi:10.1016/j.memsci.2012.01.030

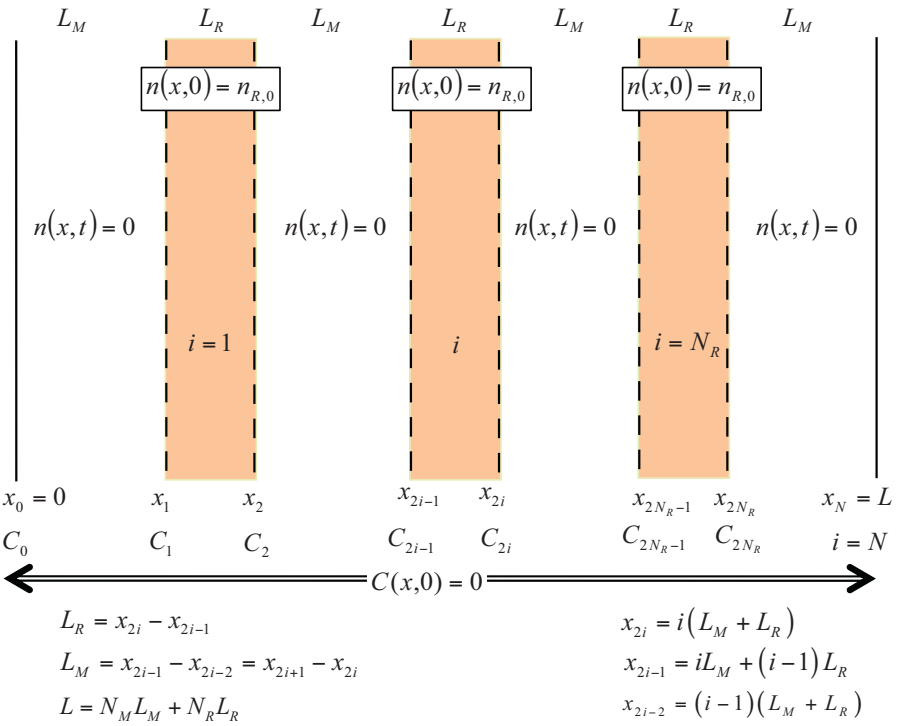

Fig. 1. Schematic of layered polymer barrier material. There are N_M inert matrix layers of thickness L_M alternating with N_R reactive layers of thickness L_R. Reactive sites are only present in reactive layers (initial concentration $n_{R,0}$).

The index i represents each adjacent pair of inert matrix and reactive layers, where the position of the inert matrix layer is given by $x_{2i-2} < x < x_{2i-1}$, $i = 1, 2, 3..., N_R + 1$ and the position of the reactive layer is given by $x_{2i-1} < x < x_{2i}$, $i = 1, 2, 3..., N_R$. The constant thickness of each reactive layer is given by $L_R = x_{2i} - x_{2i-1}$ and the constant thickness of each inert layer is given by $L_M = x_{2i-1} - x_{2i-2}$.

The one-dimensional transient transport in the layered film can be described by the material balances for oxygen and reactive sites over the whole film. The concentration of reactive sites $n(x, t)$ in the inert matrix layers is zero at all times, and the initial concentration of reactive sites is given by $n_{R,0}$ for all reactive layers. Thus,

$$n(x, t) = 0, \quad x_{2i-2} < x < x_{2i-1},\ i = 1, 2, 3..., N_R + 1, \tag{1}$$

$$n(x, 0) = n_{R,0}, \quad x_{2i-1} < x < x_{2i},\ i = 1, 2, 3..., N_R. \tag{2}$$

For packaging applications, the upstream boundary is typically exposed to air and the downstream boundary is exposed to vanishingly small oxygen partial pressure. Initially, all reactive sites in the reactive layers are available and the whole film (inert and reactive layers) is devoid of oxygen. The material balances for the concentration of oxygen $C(x, t)$ and reactive sites $n(x, t)$ and the initial and boundary conditions are given by

$$\frac{\partial C}{\partial t} = \frac{\partial}{\partial x}\left[D(x)\frac{\partial C}{\partial x}\right] - k_R\, Cn, \tag{3}$$

$$\frac{\partial n}{\partial t} = -\ \hat{\nu}\, k_R\, C\, n, \tag{4}$$

$$\text{I.C.} : C(x, 0) = 0, \tag{5}$$

$n(x, 0) = 0$ or $n_{R,0}$ depending on whether the layer is reactive or not, and

$$\text{B.C.} : C(0, t) = C_0,\ C(L, t) = 0, \tag{6}$$

where x is the position along the thickness of the film, t is time, D is the oxygen diffusion coefficient, k_R is the reaction rate constantand $\hat{\nu}$ is the stoichiometric coefficient for the scavenging reaction. The concentration $C_o = S_M p_o$ where p_o is the partial pressure of oxygen in the adjacent gas phase and is taken throughout this paper as 0.21 atm. The diffusion coefficient for each layer is assumed to be constant, where $D(x) = D_R$ is the diffusion coefficient for the reactive layers, and $D(x) = D_M$ is the diffusion coefficient for the inert matrix layers. It is assumed that oxidation of the reactive layers does not change the oxygen permeability of this material. We have observed experimentally that oxidation can change the permeability of these layers by a lot; it can be decreased by perhaps two orders of magnitude. This issue will be addressed in subsequent versions of the model. This effect will make the layered systems even better barriers and will affect some of the conclusions on comparisons of the layered structures with blends.

At the interfaces between reactive and inert matrix layers the flux and the oxygen partial pressure p_i are continuous, but the oxygen concentration on the reactive and inert sides obey the equilibrium partitioning relation given by $p_i = C_{M,i}/S_M = C_{R,i}/S_R$, where S_M is the solubility coefficient for oxygen in the inert matrix and S_R is the solubility coefficient for oxygen in the reactive layer.

The oxygen flux at the downstream boundary and the total amount of oxygen permeated are quantities of interest derived from the solution of Eqs. (3)–(6). The downstream flux $J\big|_{x=L}$ at time t is given by

$$J\big|_{x=L} = -\left(D\frac{\partial C}{\partial x}\right)\bigg|_{x=L}, \tag{7}$$

and the total amount of oxygen permeated per unit area of the membrane or cumulative permeate Q_t at time t is given by

$$Q_t = \int_0^t J\big|_{x=L}\, dt. \tag{8}$$

Table 1
List of parameters for the multilayer base case calculations.

Symbol	Name	Value
L	Total film thickness	0.025 cm
ϕ	Volume fraction of reactive layers in film	0.1
$n_{R,0}$	Initial concentration of reactive sites in reactive layers	8000 $\mu mol_{RS}/cm^3$
$\hat{\nu}$	Stoichiometric coefficient	2 $\mu mol_{RS}/\mu mol_{O_2}$
S_M	Oxygen solubility coefficient for the inert matrix layers	4.38 $\mu mol_{O_2}/cm^3$ atm
D_M	Oxygen diffusion coefficient for the inert matrix layers	4.84×10^{-4} cm^2/day
S_R	Oxygen solubility coefficient for the reactive layers	4.38 $\mu mol_{O_2}/cm^3$ atm
D_R	Oxygen diffusion coefficient for the reactive layers	1.73×10^{-4} cm^2/day
k_R	Reaction rate coefficient	0.42 $cm^3/\mu mol_{RS}$ day

3. Parametric study

The material balances and initial and boundary conditions (Eqs. (3)–(6)) were solved numerically using an explicit finite difference method. The equations were discretized using a two-point forward difference for the time derivatives and a three-point central difference for the spatial derivatives. While the numerical solution was developed in MATLAB for convenient matrix manipulation, it did not rely on any specialized solvers. The equilibrium and flux boundary conditions were enforced at each interface. Table 1 lists the parameters used for the base case calculations, which were taken from Ferrari et al. [1] and the sources referenced therein. Variations from these parameters are indicated with results when appropriate. The downstream oxygen flux defined by Eq. (7) and the cumulative permeate defined by Eq. (8) are plotted versus time for various cases. The results are organized in two categories: (1) effects of layer configuration and (2) effects of physical parameters on barrier properties, as discussed in the next sections.

3.1. Effect of layer configuration on transient barrier performance

Fig. 2 presents the results for the base case (parameters given in Table 1) and illustrates the effects of total number of layers for films where the first and last layers are inert and the total number of layers is odd. This is a likely configuration for packaging applications, as the scavenging material may be encapsulated between inert layers. In the figure labels an inert matrix layer is represented by 0 and a reactive layer is represented by 1. Fig. 2 shows the transient downstream flux and the cumulative oxygen permeate.

The vertical dashed lines in Fig. 2 represent the time lag calculated from the numerical solutions, which is independent of the number of layers. The transient flux and consequently the oxygen permeate prior to the time lag, however, are quite dependent on the number of layers. The initial flux plateau is about ten times lower for a film with a total of seven layers (0 1 0 1 0 1 0) compared to a film of three layers (0 1 0). At intermediate times, the fluxes cross over, with the flux in the three-layer film being lowest, until all the fluxes merge into the same steady state values. Fig. 2b shows the oxygen permeate on the same time scale for easy comparison, showing a much less pronounced difference after the crossover point. Note that the cross-over time is ~100 days, and time lag is ~300 days, thus the choice of additional layers may be advantageous when very low oxygen exposure is preferable at the early portion of the product life, particularly since the exposure at intermediate times is comparable. It should be noted that despite log scale, the duration of the plateau phase is relatively short compared to the time lag. The waviness in the flux and cumulative flux curves is because the travelling concentration wave is moving repeatedly from reactive to inert layers.

Fig. 3 shows the transient downstream flux and cumulative oxygen permeate for even total number of layers. The time lag is largest for the configuration 01 (i.e., first layer inert, second layer reactive) and smallest for configuration 10. This is because making the first layer inert lowers the concentration of oxygen in the reactive layer, extending its life, as noted by Nuxoll et al. [12]. As the number of layers increase, the order of the layers becomes less important, and eventually films with first layer inert or reactive will have the same time lag. The value of the initial flux plateau is only affected by the total number of layers, but as can be seen in Fig. 3a, the duration of the plateau flux is much longer for films where the first layer is inert. Similar to the configurations discussed in Fig. 2, there is a crossover point where the initially lower flux and permeate (Fig. 3b) for the 0101 configuration becomes large enough to surpass the 01 film. For the films with the first layer reactive, this crossover point is not observed, making 1010 configuration better than 10 configuration at all times.

Fig. 4a compares the downstream flux for films with configuration 0 and 101. While the time lag and the steady-state flux are the same for both films, the 101 configuration consistently has

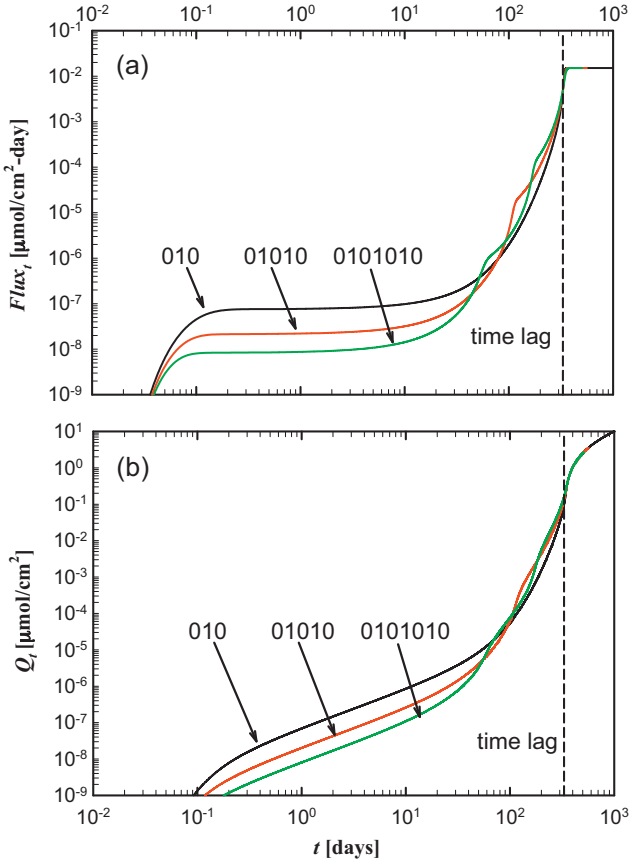

Fig. 2. (a) Downstream flux and (b) oxygen permeate versus time in log-log scale. Layer sequence for each case indicated in chart, where 0 represents an inert layer, and 1 represents a reactive layer. All configurations shown have odd total number of layers. The dashed vertical line indicates time lag θ calculated from the numerical solution. All cases shown use the parameter values given in Table 1.

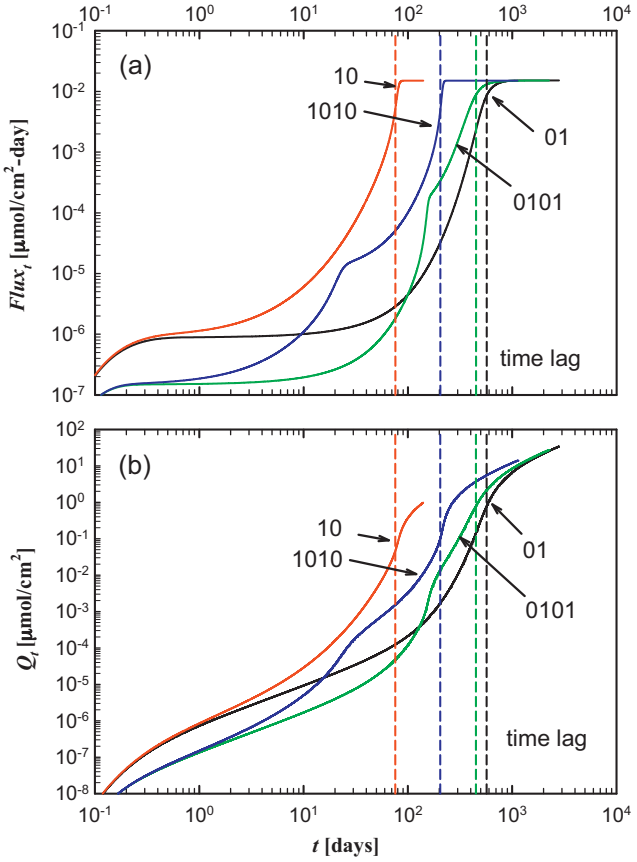

Fig. 3. (a) Downstream flux and (b) oxygen permeate versus time in log-log scale. Layer sequence for each case indicated in chart, where 0 represents an inert layer, and 1 represents a reactive layer. All configurations shown have even total number of layers. The dashed vertical line indicates time lag θ calculated from the numerical solution. All cases shown use the parameter values given in Table 1.

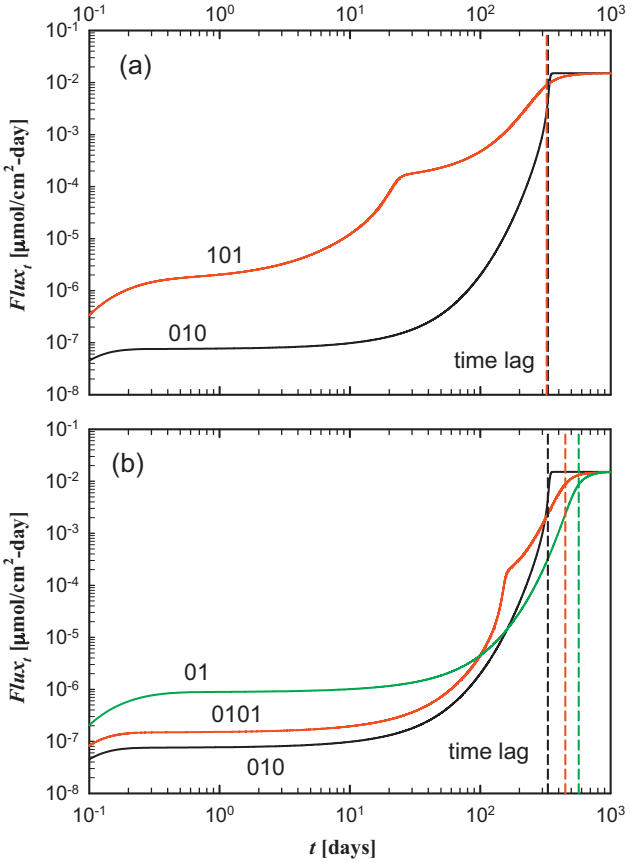

Fig. 4. Downstream flux versus time for various layer configurations. Layer sequences for each case are indicated in chart, where 0 represents an inert layer, and 1 represents a reactive layer. The dashed vertical lines represent time lag θ calculated from the numerical solution by extrapolating the asymptote $Q_{t\to\infty}$ to the time axis. All cases shown use the parameter values given in Table 1.

higher flux than 010. Fig. 4b compares configuration 010 to 01 and 0101. Both 01 and 0101 have larger time lags(desirable) than 010. However, the flux for 0101 is higher than for 010 until very near steady state. For applications that tolerate higher flux early on, the extended time lag of 01 may be attractive.

Table 2 summarizes the layer configurations discussed in Figs. 2–4, along with key results. N_M is the number of inert matrix layers, each of thickness L_M. Similarly, N_R is the number of reactive layers, each of thickness L_R. There are many trade-offs in the selection of the ideal layer configuration, as there are no combinations that give both the largest time lag and the smallest flux plateau. One key example is shown in Fig. 4b: even though the time lag for 0101 is 120 days longer than for 010, the lower downstream flux of 010 for most of its useful life probably makes it a better choice than 0101.

In general layer configurations where the first layer is inert outperform (i.e., have lower flux prior to time lag) configurations where the first layer is reactive. Furthermore, if very low initial flux is desirable at the expense of shorter life times, configurations with odd total number of layers are preferable, and increasing the number of layers reduces the plateau flux further. On the other hand, if the goal is very long duration and a moderate plateau flux is tolerated, then configuration 01 may be considered. Note, however, that for food and drug applications, it is probably preferable to avoid contact between the scavenging layer and the product, and thus 01 would not be a good practical choice.

3.2. Effect of physical parameters on barrier properties

Unless noted, the results in this section are given for layer configuration 010, i.e., a reactive layer between two inert matrix layers. The parameters values given in Table 1 are used as the base case, and variations are indicated with each result. Fig. 5a shows the transient downstream flux for varying $\Delta = D_R/D_M$ with $D_M = 4.84 \times 10^{-4}$ cm^2/day held fixed. Fig. 5b shows the oxygen permeate versus time on a linear scale for the same films shown in Fig. 5a. Reducing Δ modestly reduces the steady-state flux, but it reduces the initial flux plateau by orders of magnitude. As illustrated in figure Fig. 5b, reducing Δ increases time lag with a highly non-linear dependence, as evidenced by the large increase caused by changing Δ from 0.36 to 0.17 compared to the modest increase caused by changing Δ from 3 to 1.

Fig. 6 compares (a) the initial flux plateau and (b) the time lag for various combinations of Δ and volume fraction ϕ. The values were obtained by numerical solution of Eqs. (3)–(6), but also agree with the analytical predictions discussed in the next section. Increasing the volume fraction ϕ significantly decreases the flux plateau and increases the time lag, especially for smaller values of Δ. As the results of Figs. 5 and 6 show, the barrier performance of a multilayer system is significantly dependent on Δ, particularly if $\Delta < 1$. The effect of Δ on time lag and initial flux plateau are both related to the effect of Δ on the diffusion time scale. Decreasing Δ increases the diffusion time scale and increases the exposure of oxygen to the reactive sites, leading to more complete reaction and reducing the

Table 2
Comparison of time lag θ and initial flux plateau J_{pl} obtained from the numerical solutions for several layer configurations. Layer sequence for each case indicated in table, where 0 represents an inert layer, and 1 represents a reactive layer. All cases use the parameter values given in Table 1.

Layer sequence	N_M	N_R	L_M (μm)	L_R (μm)	θ (day)	J_{pl} (μmol/cm^{2}day)
0 1	1	1	225	25	570	1×10^{-6}
1 0	1	1	225	25	76	1×10^{-6}
0 1 0	2	1	112.5	25	331	7.3×10^{-8}
1 0 1	1	2	225	12.5	323	1.5×10^{-6}
0 1 0 1	2	2	112.5	12.5	450	1.5×10^{-7}
1 0 1 0	2	2	112.5	12.5	204	1.5×10^{-7}
0 1 0 1 0	3	2	75	12.5	331	2.1×10^{-8}
0 1 0 1 0 1 0	4	3	56.25	8.33	331	8.2×10^{-9}

initial flux plateau. Time lag is proportional to diffusion time scale, therefore decreasing Δ increases time lag.

Fig. 7 shows the downstream flux versus time for varying $H = S_M/S_R$ for fixed $S_M = 4.38\ \mu mol_{O_2}/cm^3$ atm with Δ = 1 for Fig. 7a and Δ = 0.357 for Fig. 7b. Decreasing H decreases the initial flux plateau, which is a desirable trend, even though it causes the steady-state flux to increase. However, decreasing H also decreases time lag, which is undesirable. Decreasing Δ reduces the sensitivity of H on the initial flux plateau and increases it on time lag and steady-state flux. This is because higher oxygen solubility within the reactive layers increases the amount of oxygen available to react with the scavenging sites.

Fig. 8 compares the effect of H on (a) the initial flux plateau and (b) the time lag in log scale for three layer configurations with Δ = 1 and 0.357, as shown in the charts. The values were obtained by numerical solution of Eqs. (3)–(6) and generally agree with the analytical predictions discussed in the next section. As shown in Fig. 8a, reducing Δ reduces the effect of H and of the number of layers in the initial flux plateau. Fig. 8b shows that time lag has a linear dependence on H. Since the time lag does not depend on the number of layers when the total number is odd, only one curve is shown for each value of Δ.

4. Analysis of early times to predict flux plateau

At early times most reactive sites are still available, and a quasi-steady-state region is observed for the downstream oxygen flux (e.g., Fig. 2a), called the flux plateau. Approximate analytical solutions to predict the initial flux plateau for homogeneous reactive

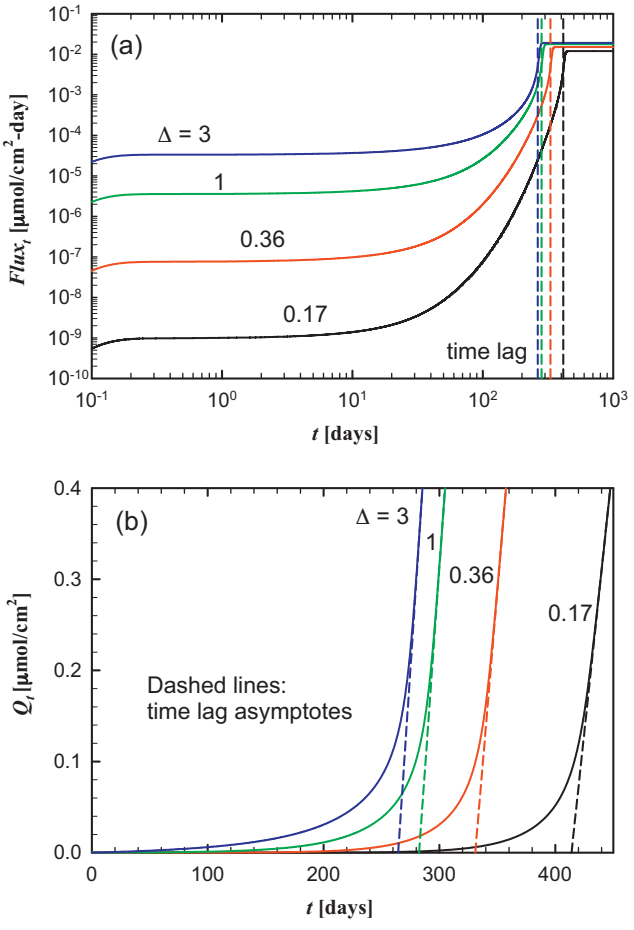

Fig. 5. (a) Downstream flux versus time on a log-log scale and (b) permeate versus time on a linear scale for a film with three layers, with the first and last inert, varying Δ (with $D_M = 4.84\times10^{-4}$ cm^2/day held fixed) as indicated in charts. All other parameter values are given in Table 1. The dashed lines indicate the time lag θ calculated from the numerical solution.

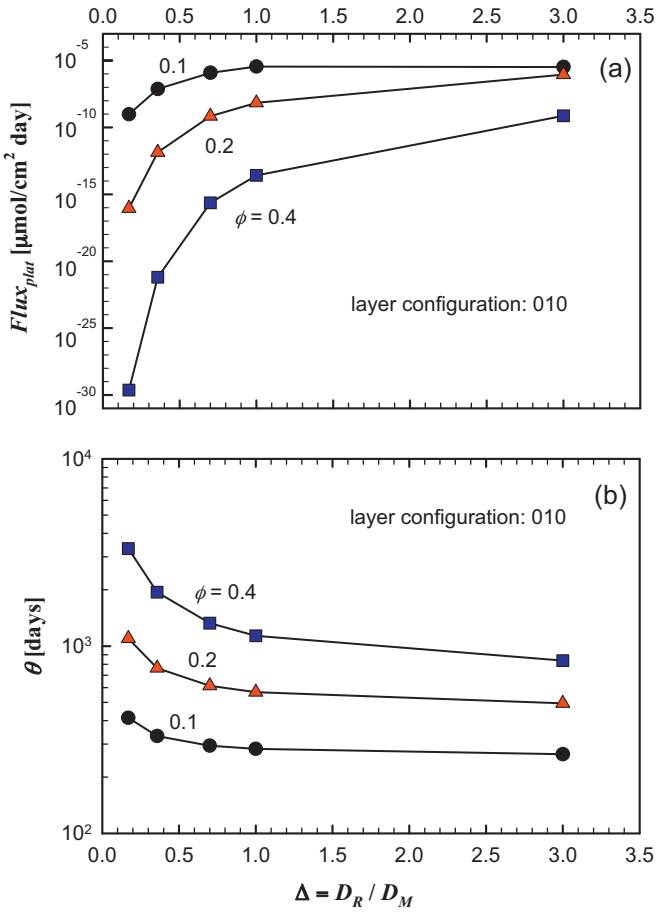

Fig. 6. Effect of Δ (with $D_M = 4.84\times10^{-4}$ cm^2/day held fixed) and volume fraction ϕ on (a) initial downstream flux plateau and (b) time lag for a film with three layers. All other parameter values are given in Table 1. The values for flux plateau and time lag were obtained from numerical solution of Eqs. (3)–(5).

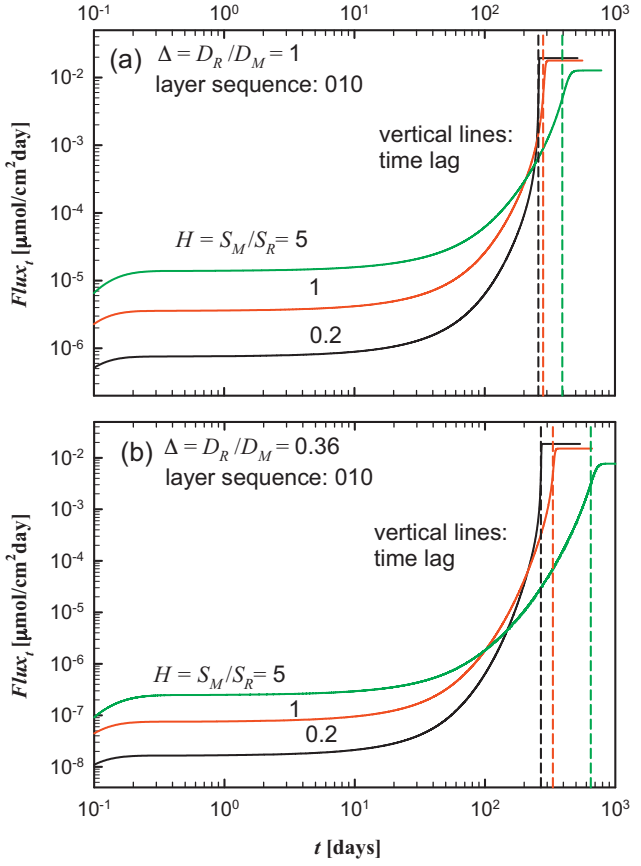

Fig. 7. Downstream flux versus time for a film with three layers, with the first and last inert, varying H as indicated in charts. (a) $\Delta = 1$, (b) $\Delta = 0.357$ (with $D_M = 4.84 \times 10^{-4}$ cm²/day and $S_M = 4.38\ \mu mol_{O_2}/cm^3$ atm held fixed). All other parameter values are given in Table 1. The vertical dashed lines indicate the time lag θ calculated from the numerical solution by extrapolating the asymptote $Q_{t\to\infty}$ to the time axis.

membranes have been derived by Carranza et al. [2]. Here, a similar analysis is utilized for each reactive layer and combined with transport in the inert matrix layers to derive a system of equations for the layered film. Consider a multilayer film with inert material at both its upstream and downstream ends. The transport equations for the inert matrix layers reduce to steady state one-dimensional diffusion,

$$D_M \frac{d^2 C_M}{dx^2} = 0, \quad x_{2i-2} < x < x_{2i-1},\ i = 1, 2, 3\ldots, N_R + 1, \tag{9}$$

where C_M is the oxygen concentration within the inert matrix layer. At early times most reactive sites are still available within the reactive layers,

$$n(x) \approx n_{R,0}, \quad x_{2i-1} < x < x_{2i}, \quad i = 1, 2, 3\ldots, N_R. \tag{10}$$

The transport equations reduce to an equivalent steady-state first order reaction equation,

$$\frac{d^2 C_R}{dx^2} - \alpha^2 C_R = 0, \tag{11}$$

where C_R is the oxygen concentration within the reactive layer and $\alpha = \sqrt{k_R\, n_{R,0}/D_R}$.

At the interfaces between reactive and inert matrix layers, the flux and oxygen partial pressure are continuous, but the oxygen concentration on the reactive and inert sides obey the partition relation $p_i = C_{M,i}/S_M = C_{R,i}/S_R$, where S_M is the solubility coefficient for oxygen in the inert matrix and S_R is the solubility coefficient for oxygen in the reactive layer. The flux evaluated at the upstream layer boundary x_{2i-1} of a reactive layer i must equal the flux from the inert layer bound by $x_{2i-2} < x < x_{2i-1}$,

$$J\big|_{x_{2i-1}} = \underbrace{\frac{-\alpha D_R S_R\,[p_{2i} - p_{2i-1}\cos h(\alpha L_R)]}{\sin h(\alpha L_R)}}_{\text{reactive}} = \underbrace{\frac{-D_M S_M}{L_M}(p_{2i-1} - p_{2i-2})}_{\text{inert}}. \tag{12}$$

Likewise, the flux evaluated at the downstream boundary x_{2i} of the same layer must equal the flux into the inert matrix layer bound by $x_{2i} < x < x_{2i+1}$,

$$J\big|_{x_{2i}} = \underbrace{\frac{-\alpha D_R S_R\,[p_{2i}\cos h(\alpha L_R) - p_{2i-1}]}{\sinh(\alpha L_R)}}_{\text{reactive}} = \underbrace{\frac{-D_M S_M}{L_M}(p_{2i+1} - p_{2i})}_{\text{inert}}. \tag{13}$$

The complete system of equations to solve the initial flux plateau is given by Eqs. (12) and (13) written for $i = 1$ to $i = N_R$, which in matrix form becomes

$$\begin{bmatrix} b & -c & 0 & \cdots & 0 & 0 & 0 \\ -c & b & -a & \cdots & 0 & 0 & 0 \\ 0 & -a & b & \cdots & 0 & 0 & 0 \\ 0 & 0 & -c & \cdots & 0 & 0 & 0 \\ \vdots & \vdots & \vdots & \ddots & \vdots & \vdots & \vdots \\ 0 & 0 & 0 & \cdots & -a & b & -c \\ 0 & 0 & 0 & \cdots & 0 & -c & b \end{bmatrix} \begin{bmatrix} p_1 \\ p_2 \\ p_3 \\ p_4 \\ \vdots \\ p_{2N_R-1} \\ p_{2N_R} \end{bmatrix} = \begin{bmatrix} a\,p_{O_2} \\ 0 \\ 0 \\ 0 \\ \vdots \\ 0 \\ a\,p_N = 0 \end{bmatrix}. \tag{14}$$

Recall that the oxygen partial pressure at the downstream boundary is 0 for this problem, i.e., $p_N = p_L = 0$. Since the last layer is inert, the downstream oxygen flux for early times is given by

$$J\big|_L = \frac{-D_M}{L_M}(C_{M,N} - C_{M,2N_R}) = \frac{D_M C_{M,2N_R}}{L_M} = \frac{S_M D_M}{L_M} p_{2N_R}. \tag{15}$$

Note that only the oxygen partial pressure at x_{2N_R} is required for the calculation of the downstream flux. The linear system defined by Eq. (15) was solved analytically using Mathematica for various N_M and N_R, giving expressions for predicting the downstream flux at early times. The full analytical solution includes a denominator consisting of multiple exponential terms and pre-factors. However, in the limit of $\Phi_R \gg 1$, where $\Phi_R = \sqrt{(L_R N_R)^2 k_R\, n_{R,0}/D_R}$ is the Thiele modulus for the reactive layers, the initial flux plateau is given by,

$$J\big|_L = \frac{2^{N_R} H^{N_M-1} D_M{}^{N_M} \alpha D_R S_M p_{O_2} e^{-\Phi_R}}{(HD_M + \alpha D_R L_M)^{N_M - N_R + 1}(2HD_M + \alpha D_R L_M)^{N_R - 1}}, \tag{16}$$

where $\alpha = \sqrt{k_R n_{R,0}/D_R}$ and $H = S_M/S_R$ is the oxygen partition coefficient between inert and reactive layers. In order to evaluate the flux dependence on the number of layers for an equivalent loading of scavenger material, the individual layer thickness can be expressed in terms of the volume fraction of reactive polymer, ϕ, and the total thickness of the film, L, making $L_R = \phi L/N_R$ and $L_M = (1-\phi)L/N_M$. The leading order estimate for the downstream flux plateau for early times thus becomes

$$J_{pl} = \frac{2^{N_R} \Delta D_M S_M p_{O_2} \Phi_R e^{-\Phi_R}}{H\phi L(1 + \gamma/N_M)^{N_M - N_R + 1}(2 + \gamma N_M)^{N_R - 1}}, \tag{17}$$

where $\gamma = \Phi_R \Delta(1-\phi)/\phi H$, $\Delta = D_R/D_M$ and $\Phi_R = \sqrt{(\phi L)^2 k_R n_{R,0}/D_R}$. While Eq. (17) for the downstream flux was derived assuming the first layer of the film is inert matrix, this analytical expression is valid for any odd or even number of layers, either starting with inert matrix or with reactive layer, and by entering the proper number of reactive and inert layers (N_R, N_M).

Table 3 summarizes how well the leading order estimate for the flux plateau (Eq. (17)) approximates the full solution of Eq. (14) for various Δ and k_R for films with a total of 5 and 20 layers, as indicated in table. The upstream layer is inert in both cases and there is an inert or reactive downstream layer for the

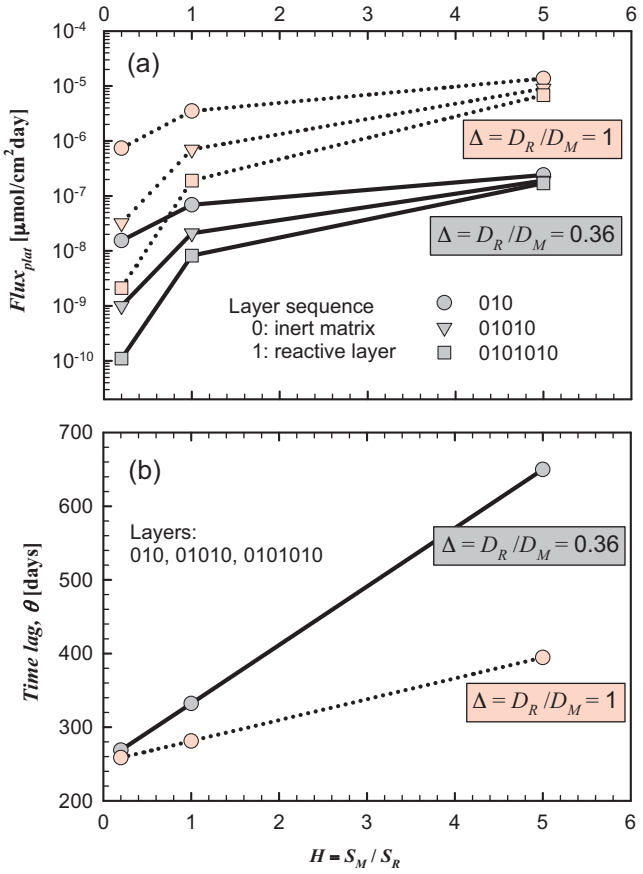

Fig. 8. Effect of H and Δ (with $D_M = 4.84 \times 10^{-4}$ cm²/day and $S_M = 4.38\ \mu mol_{O_2}/cm^3$ atm held fixed) on (a) initial downstream flux plateau and (b) time lag for films with layer configurations 010, 01010, 0101010, where 0 represents an inert matrix layer and 1 represents a reactive layer. All other parameter values are given in Table 1. The values for flux plateau and time lag were obtained from numerical solution of Eqs. (3)–(6).

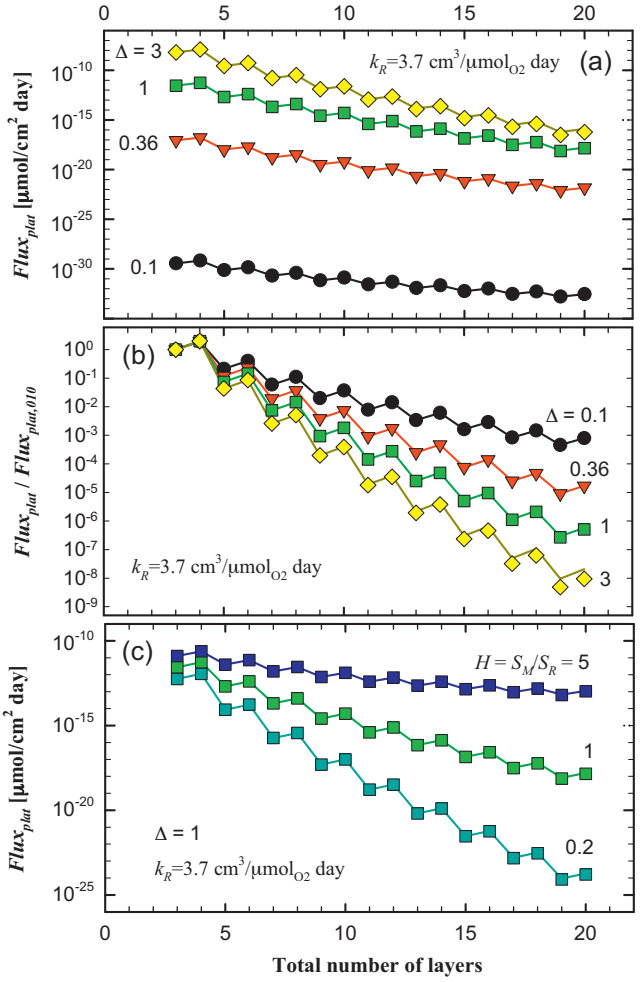

Fig. 9. Flux plateau estimate versus total number of layers. Symbols: leading order estimate. Solid lines: estimate based on full solution of Eq. (14). For all cases $L = 0.025$ cm, $C_0 = 0.92\ \mu mol_{O_2}/cm^3$, $D_M = 4.84 \times 10^{-4}$ cm²/day, k_R is $3.7\ cm^3/\mu mol_{RS}$ day. For (a) and (b) $H = 1$, with Δ varying as indicated (with $D_M = 4.84 \times 10^{-4}$ cm²/day and $S_M = 4.38\ \mu mol_{O_2}/cm^3$ atm held fixed). For (c) $\Delta = 1$ with H varying as indicated. The flux plateau in (b) is normalized by the flux plateau for a film of 010 configuration.

5 or 20 layer system, respectively. The comparison is made in terms of the ratio $J_{pl,\ leading\ order}/J_{pl,\ solution\ Eq.\ (14)}$, thus a value of unity means perfect agreement. For all cases shown, the predictions were evaluated for a multilayer membrane of total thickness $L = 0.025$ cm, reactive polymer volume fraction $\phi = 0.1$, with PET as the inert matrix polymer (i.e., $D_M = 4.84 \times 10^{-4}$ cm²/day, $C_0 = S_M p_{O_2} = 0.92\ \mu mol_{O_2}/cm^3$) and assuming the partition coefficient $H = 1$. In general, the agreement between both predictions is best for smaller Δ, smaller number of layers and larger k_R. The agreement between the leading order prediction and the full solution of Eq. (14) becomes poor for a combination of small k_R, large Δ and large number of layers, as illustrated by the case of 20 layers, $\Delta = 3$ and $k_R = 0.42\ cm^3/\mu mol_{RS}$. This is not surprising, since the leading order prediction assumes that $\Phi_R \gg 1$ to discard lower order exponential terms, but if the rate constant is $k_R = 0.42\ cm^3/\mu mol_{RS}$ and $\Delta = 1$ and 3 the values of Φ_R are 6.5 and 3.8, respectively.

Table 3
Ratio between leading order estimate of the flux plateau (Eq. (17)) and the flux plateau estimate based on the full solution of Eq. (14). Results shown for films with 5 and 20 total number of layers for various Δ and k_R, as indicated. The upstream layer is inert in all cases and there is an inert or reactive downstream layer for the 5 or 20 layer system, respectively. All other parameters are given in Table 1.

Number of layers	k_R ($cm^3/\mu mol_{RS}$ day)	$J_{pl,\ leading\ order}/J_{pl,\ solution\ Eq.(14)}$			
		$\Delta = 0.1$	$\Delta = 0.357$	$\Delta = 1$	$\Delta = 3$
5	0.42	1.00	1.00	1.00	0.96
20	0.42	0.98	0.70	0.27	0.04
5	3.7	1.00	1.00	1.00	1.00
20	3.7	1.00	0.99	0.88	0.46
5	10.3	1.00	1.00	1.00	1.00
20	10.3	1.00	1.00	0.99	0.84

Fig. 9a shows the initial flux plateau predictions versus the total number of layers for films with the first layer inert for various Δ, as indicated in chart. Solid lines represent the estimate based on the full analytical solution of Eq. (14); symbols represent the leading order solution, given by Eq. (17). For all cases shown, the predictions were evaluated for a multilayer membrane of total thickness $L = 0.025$ cm, reactive polymer volume fraction $\phi = 0.1$, reaction rate constant $k_R = 3.7\ cm^3/\mu mol_{RS}$, with PET as the inert matrix polymer (i.e., $D_M = 4.84 \times 10^{-4}$ cm²/day, $C_0 = S_M p_{O_2} = 0.92\ \mu mol_{O_2}/cm^3$) and assuming the partition coefficient $H = 1$. Fig. 9b shows the flux estimates for the same cases shown in Fig. 9a, except that the flux plateau is normalized by the flux plateau for layer configuration 0 1 0 (0 represents inert matrix layer, 1 represents reactive layer). While the absolute value of the initial flux plateau decreases with Δ by orders of magnitude, as seen in Fig. 9a, larger values of Δ lead to greater reduction in the initial flux plateau by increasing the number of layers, as shown in Fig. 9b.

Fig. 9c explores the effect of varying H when $\Delta = 1$ for the same layer configuration and parameters used in Fig. 9a. Solid lines represent the estimate based on the full analytical solution of Eq. (14);

symbols represent the leading order solution, given by Eq. (17). Decreasing H magnifies the effect of total number of layers in the flux plateau, as illustrated in Fig. 9c.

The effects of Δ, H, and k_R, may be explained by inspection of the parameter groups $\Phi_R = \sqrt{(\phi L)^2 k_R n_{R,0}/D_R}$ and $\gamma = \Phi_R \Delta(1-\phi)\phi H$ in Eq. (17). Decreasing Δ causes Φ_R to increase, thus reducing the initial flux plateau. However, decreasing Δ also causes γ to decrease, thus reducing the effect of the number of layers on the initial flux plateau. Decreasing H causes γ to increase, thus magnifying the effect of number of layers on the initial flux plateau. Finally, increasing k_R increases both Φ_R and γ, thus decreasing the initial flux plateau and magnifying the effect of number of layers on the plateau value.

As illustrated in Fig. 9 and discussed above, when all other parameters are kept the same, increasing the number of layers causes the initial flux plateau to decrease. While parameters such as Δ, H, and k_R may magnify or diminish the effect of number of layers on the flux plateau, the trend is valid for all cases. The physical interpretation of this observation lies on the effective increase of length of the reactive region when the number of layers is increased. Looking at layer sequence 010, where 0 represents inert matrix layer and 1 represents a reactive layer, all reaction takes place in the continuous region of thickness $L_R = \phi L$. On the other hand, a film with layer sequence 01010 has an inert matrix layer of thickness $L_M = (1-\phi)L/3$ between the two reactive layers, slowing down oxygen transport and thus increasing contact time between oxygen and scavenging sites at the second reactive layer. For a film with N_M inert matrix layers (where the first and last layers are inert), the reaction region is increased to $L - 2L_M = L - 2(1-\phi)/N_M$, thus the larger the number of layers, the longer the oxygen diffusion path between reactive layers, causing the initial flux plateau to decrease. Note that this comparison is only meaningful for similar configuration types: i.e., a film with configuration 010 must be compared to films with configuration 01010, 0101010, and so on. Likewise, a film with configuration 01 must be compared to films with configuration 0101, 010101, etc.

5. Steady state analysis

At long times most reactive sites have been consumed and the steady-state downstream flux is constant and given by $J_{SS} = P(p_{O_2,0} - p_{O_2,L})/L$, where P is the effective permeability of the composite, which is obtained by the well-known additive relation between the resistance to flux in each layer [16],

$$\frac{L}{P} = \sum_{i=1}^{N} \frac{L_i}{P_i} = N_R \frac{L_R}{P_R} + N_M \frac{L_M}{P_M}, \tag{18}$$

where $P_M = S_M D_M$ and $P_R = S_R D_R = S_M D_M \Delta/H$. Since the downstream pressure $p_{O_2,L}$ is vanishingly small, using $L_R = \phi L/N_R$ for reactive layer thickness and $L_M = (1-\phi)L/N_M$ for inert layer thickness, the steady-state flux is given by

$$J_{SS} = \frac{P p_{O_2}}{L} = \frac{\Delta D_M S_M p_{O_2}}{L[\phi H + \Delta(1-\phi)]}. \tag{19}$$

The steady-state flux given by Eq. (19) is valid for any layer configuration and values of $\Delta = D_R/D_M$ and $H = S_M/S_R$.

Time lag is calculated by extrapolating the steady-state oxygen permeate to cross the time axis, i.e., the time when $Q_{t\to\infty} = 0$. To obtain an analytical expression (e.g. [1,11]), all layers are set to have same diffusion coefficient and the same solubility coefficient, i.e., $D_R = D_M$ and $S_R = S_M$. Combining the oxygen material balance and the reactive sites material balance for the entire film (Eqs. (3) and (4)) gives

$$\frac{\partial C}{\partial t} - \frac{1}{\hat{\nu}} \frac{\partial n}{\partial t} = D_M \frac{\partial^2 C}{\partial x^2}. \tag{20}$$

and the time lag θ is given by

$$\theta_{\Delta=1,H=1} = \frac{L^2}{6D_M} + \frac{1}{D_M C_0 \hat{\nu}} \int_0^L x n_{t=0} dx, \tag{21}$$

where C_0 is the oxygen concentration at the upstream boundary, $\hat{\nu}$ is the stoichiometric coefficient for the scavenging reaction and $n_{t=0}$ is the initial concentration of reactive sites along the entire film. Eq. (21) is valid for either a homogeneous or a layered film with any layer configuration, as long as the diffusion coefficients and the solubility coefficients are the same for all layers. The details of the layer configuration must be defined to compute $n_{t=0}$ and complete the calculation of time lag.

For the inert matrix layers, the concentration of reactive sites is always 0, so only the reactive layers need to be computed. Assuming the first layer is inert matrix, the integral term containing the initial concentration of reactive sites is given by

$$\begin{aligned} \int_0^L x n_{t=0} dx &= \sum_{i=1}^{N_R} \int_{(i-1)L_R + iL_M}^{i(L_M+L_R)} x n_{R,0} dx \\ &= \frac{n_{R,0}}{2} N_R L_R \left[(N_R+1)L_M + N_R L_R\right], \end{aligned} \tag{22}$$

where $n_{R,0}$ is the initial concentration of reactive sites in each reactive layer. The summation can be evaluated, giving the closed form result for the integral. Thus, the time lag prediction for a multilayer system with odd total number of layers, θ_{odd}, is given by

$$\frac{\theta_{\text{odd},H=1,\Delta=1}}{\theta_0} = \frac{3}{\nu} + 1, \tag{23}$$

and for an even total number of layers θ_{even} becomes,

$$\frac{\theta_{\text{even},H=1,\Delta=1}}{\theta_0} = \frac{3}{\nu} \frac{(1-\phi+N_M)}{N_M} + 1, \tag{24}$$

where $\nu = S_M p_{O_2} \hat{\nu}/\phi n_{R,0}$ and $\theta_0 = L^2/6D_M$ is the diffusion time lag of the film, i.e. the time lag of the film without any reactive particles. When the first layer is reactive, $\int_0^L x n_{t=0} dx$ is computed using the proper layer ordering. For an odd total number of layers, Eq. (23) is valid. However, for an even total number of layers, time lag becomes

$$\frac{\theta_{\text{even, 1st reac, }H=1,\ \Delta=1}}{\theta_0} = \frac{3}{\nu}\left(\frac{\phi - 1 + N_M}{N_M}\right) + 1. \tag{25}$$

Comparing Eqs. (23)–(25), note that θ_{even} is a function of the number of layers (expressed by the number of inert layers N_M), while θ_{odd} is not. If all physical parameters remain the same, except the number of layers, the maximum value of θ_{even} is achieved for a single pair of inert and reactive layers, i.e., $N_M = 1$. Conversely, $N_M = 1$ gives the minimum value of $\theta_{\text{even, 1st reac}}$. As the number of layers increases, the value of θ_{even} decreases and the value of $\theta_{\text{even, 1st reac}}$ increases. For very large N_M the dependence vanishes, making Eq. (23) valid for all configurations when $N_M \gg 1$. The differences between Eqs. (23)–(25) is due to the position of the centroid of reactive sites in the membrane (cf. [11]); the centroid is always at the membrane center for an odd number of layers, but it is offset slightly upstream or downstream from the center with an even number of layers.

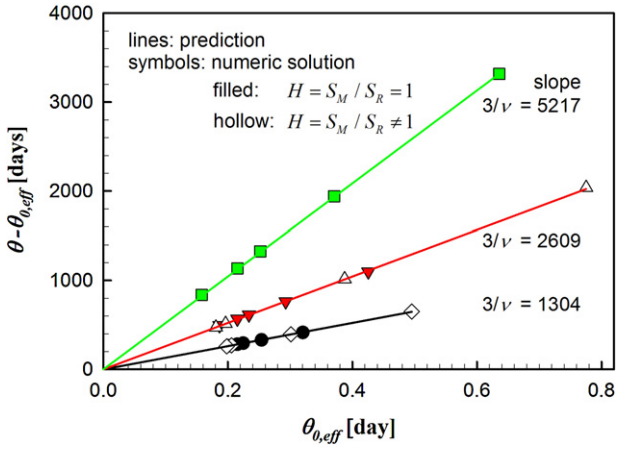

Fig. 10. Time lag for the reactive film, θ, versus the time lag for an equivalent inert layer film, $\theta_{0,\text{eff}}$. Symbols represent time lag obtained by numerical solution for a film with three layers, with inert first and last layers, Eq. (26). Parameter values are given in Table 1, except that ϕ, Δ and H varied, resulting in ν and $\theta_{0,\text{eff}}$ indicated in chart.

5.1. Prediction of time lag when the diffusion coefficient is not the same for all layers

Eqs. (23)–(25) were derived following a well-established asymptotic analysis for determination of time lag. However, the method does not easily apply to a layered system where the diffusion coefficient and/or solubility coefficient are different for reactive and inert layers. Systematic analysis of the numerical solution of Eqs. (3)–(6) (Fig. 10) resulted in the development of an equation analogous to Eq. (23) for odd total layers, but that is applicable when $\Delta \neq 1$ and $H \neq 1$. Fig. 10 shows the time lag of the reactive multilayer film versus the time lag $\theta_{0,\text{ eff}} = L^2/6D_{\text{eff}}$ for an inert film of effective diffusion coefficient $D_{eff} = \Delta D_M/[H\phi + \Delta(1-\phi)]$. The symbols represent the time lag calculated by numerical solution varying the volume fraction ϕ and the ratio between the diffusion coefficients of the reactive and inert layers Δ. The data was arranged in terms of the parameter group $\nu = S_M p_{O_2} \hat{\nu}/\phi n_{R,0}$. Symbols represent time lag calculated by numerical solution, while the solid lines represent $3\theta_{0,\text{eff}}/\nu$, indicating the time lag for odd total number of layers for $\Delta \neq 1$ and $H \neq 1$ can be predicted by

$$\frac{\theta_{\text{odd}}}{\theta_{0,\text{eff}}} = \frac{3}{\nu} + 1, \tag{26}$$

Note that when $\Delta = 1$ and $H = 1$, Eq. (26) reverts back to Eq. (23), enabling its use for both cases. Unfortunately, this approach does not extend to films where the total number of layers is even.

6. Comparison of analytical and numerical predictions

Fig. 11 compares the early-times downstream flux plateau obtained by numerical solution of Eqs. (3)–(6), and the flux plateau calculated by the leading order estimate of Eq. (17). Three layer configurations with varying combinations of ϕ, Δ and H are shown. The analytical and numerical predictions match closely.

Fig. 12 compares the time lag calculated numerically with the analytical prediction. All cases shown are for a film of configuration 0 1 0 for varying ϕ, Δ and H. Again, the analytical and numerical predictions match closely.

7. Comparison of multilayer films and polymer blends

This section compares the barrier performance of multilayer films and polymer blends, illustrated in Fig. 13, to aid in the selection of the most suitable configuration for a particular application.

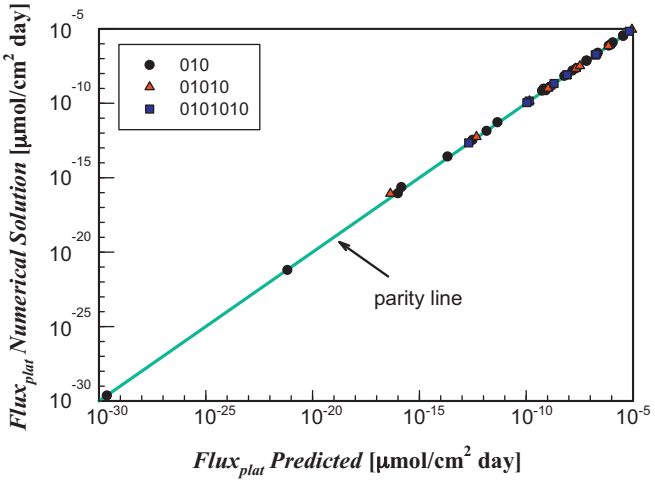

Fig. 11. Parity chart for flux plateau comparing numerical solution and analytical prediction (Eq. (17)) for three layer configurations. Layer sequence for each case indicated in chart, where 0 represents an inert matrix layer, and 1 represents a reactive layer. For all layer sequences, all permutations of $H = 0.2$, 1 and 5 with $\Delta = 0.357$ and 1 (keeping $\phi = 0.1$, $S_M = 4.38\ \mu\text{mol}_{O_2}/\text{cm}^3$ atm and $D_M = 4.84 \times 10^{-4}$ cm^2/day) are plotted. For the 0 1 0 layer sequence, all permutations of $\phi = 0.1$, 0.2 and 0.4 are plotted, with $\Delta = 0.17$, 0.357, 0.7, 1 and 3 (keeping $H = 1$ and $D_M = 4.84 \times 10^{-4}$ cm^2/day). All other parameter values are given in Table 1.

Table 4 summarizes the analytical predictions of the flux plateau and time lag for multilayer films and polymer blends [1]. Table 5 lists all parameters and values used in the comparison. As shown in Carranza et al. [2], the effective surface reaction rate k_p can be expressed in terms of k_R according to $k_p = \sqrt{D_R k_R n_{p,0}}$.

Fig. 14 compares the transient behavior of a reactive polymer blend to multilayer composites of configuration 010 and 01010, as indicated in charts. An initial flux plateau is observed for both multilayer films and polymer blends. However, rather than a smooth transition between the early times flux and the steady-state regime observed for the blend, there are intermediate inflexion points in the transient flux of the multilayer film, coinciding with the sequential exhaustion of reactive sites in each reactive layer. As discussed earlier, layering improves the early time performance of barrier films, in some cases by a few orders of magnitude. However, at intermediate times the influence of layering all but vanishes. The

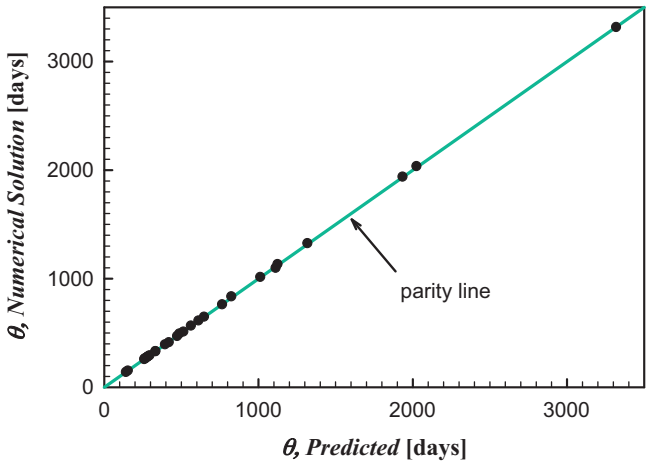

Fig. 12. Parity chart for time lag θ comparing numerical solution and analytical prediction (Eq. (26)) for a film with three layers, where the first and last layers are inert matrix. All permutations of $H = 0.2$, 1 and 5 with $\Delta = 0.357$ and 1 (keeping $\phi = 0.1$, $S_M = 4.38\ \mu\text{mol}_{O_2}/\text{cm}^3$ atm and $D_M = 4.84 \times 10^{-4}$ cm^2/day) and all permutations of $\phi = 0.1$, 0.2 and 0.4 are plotted, with $\Delta = 0.17$, 0.357, 0.7, 1 and 3 (keeping $H = 1$ and $D_M = 4.84 \times 10^{-4}$ cm^2/day). All other parameter values are given in Table 1.

Table 4
Summary of analytical prediction equations for polymer blends and multilayer reactive films.

Configuration	Initial flux plateau	Time lag
Polymer blend, spherical particles	$J_{pl} = 2J_{SS}\Phi_b e^{-\Phi_b}$, $J_{SS} = S_m p_{O_2} D_m/L$, $\Phi_b = \sqrt{3\phi k_p L^2/D_m RH}$, $H = S_m/S_p$	$\theta = \theta_0(1+3/\nu)$, $\theta_0 = L^2/6D_m$, $\nu = \hat{\nu} S_m p_{O_2}/\phi n_{p,0}$
Multilayer, first and last inert[a]	$J_{pl} = \frac{2^{N_R}\Delta D_M S_M p_{O_2}\Phi_R e^{-\Phi_R}}{H\phi L(1+\gamma/N_M)^{N_M-N_R+1}(2+\gamma/N_M)^{N_R-1}}$, $\Phi_R = \sqrt{(\phi L)^2 k_R n_{R,0}/D_R}$, $\Delta = D_R/D_M$, $\gamma = \Phi_R\Delta(1-\phi)/\phi H$, $H = S_M/S_R$	$\theta = \theta_{0,\mathrm{eff}}(1+3/\nu)$, $\theta_{0,\mathrm{eff}} = L^2/6D_{\mathrm{eff}}$, $\nu = \hat{\nu} S_M p_{O_2}/\phi n_{R,0}$, $D_{\mathrm{eff}} = \frac{\Delta D_M}{H\phi+\Delta(1-\phi)}$

[a] The flux plateau estimate shown is valid for all layer configurations. However, the time lag prediction shown is only valid for odd total layers. Time lag prediction for other layer configurations are given by Eqs. (24) and (25).

Table 5
List of parameters for comparison between homogeneous, blend and multilayer film.

Name	Symbol	Value
Total film thickness	L	0.025 cm (250 μm)
Volume fraction of reactive layers or particles	ϕ	0.1
Initial concentration of reactive sites in reactive layers or particles	$n_{R,0}$ for reactive layers $n_{p,0}$ for reactive particles	8000 $\mu mol_{RS}/cm^3$ (8×10^{-3} mol_{RS}/cm^3)
Initial concentration of reactive sites in homogeneous film	$n_0 = \phi n_{p,0}$ to match content of blend	800 $\mu mol_{RS}/cm^3$ (8×10^{-4} mol_{RS}/cm^3)
Stoichiometric coefficient	$\hat{\nu}$	2 $\mu mol_{RS}/\mu mol_{O_2}$
Oxygen solubility coefficient for the inert matrix layers or inert matrix in blend	S_M for inert matrix layer S_m for inert matrix in polymer blend	4.38 $\mu mol_{O_2}/cm^3$ atm (0.098 cm^3(STP)/cm^3 atm)
Oxygen diffusion coefficient for the inert matrix layers or inert matrix in blend	D_M for inert matrix layer	4.84×10^{-4} cm^2/day (5.6×10^{-9} cm^2/s)
Oxygen solubility coefficient for the reactive layers or particles	S_R for reactive layers	4.38 $\mu mol_{O_2}/cm^3$ atm (0.098 cm^3(STP)/cm^3 atm)
Oxygen diffusion coefficient for the reactive layers or particles	D_R for reactive layers	1.73×10^{-4} cm^2/day (2×10^{-9} cm^2/s)
Bulk reaction rate constant for reactive layers	k_R	0.42 $cm^3/\mu mol_{RS}$ day
Surface reaction rate constant for particles	$k_p = \sqrt{D_R k_R n_{p,0}}$ to match the rate for multilayer film	0.76 cm/day (8.8×10^{-6} cm/s)

time lag for the multilayer films is longer than for blends whenever $\Delta < 1$, as it is the case for Fig. 14. However, since the initial flux plateau is so much lower for the blend than the multilayer films in this particular case, the blend will outperform the layered films for most of its useful life.

Fig. 15 uses the analytical expressions for blends and multilayer films, summarized in Table 4, to compute initial flux plateau (Fig. 15a) and time lag (Fig. 15b) when Δ is varied. Only configuration 0 1 0 is presented in this comparison, which reduces the initial flux plateau prediction to

$$J_{pl} = \frac{2\Delta D_M S_M p_{O_2}\Phi_R e^{-\Phi_R}}{H\phi L(1+\gamma/2)^2}. \quad (27)$$

The multilayer flux plateau is evaluated for two bulk reaction rates (k_R = 0.42 and 4.2 $cm^3/\mu mol_{RS}$ day, as indicated). All other parameter values are the same for the blend and multilayer films and are given in Table 5. Since time lag is independent of reaction rate, for the blend the time lag is the same for all cases, and for the multilayer film, only one value is required for each Δ. Note that the blend model neglects the small contribution of the blend particles to the effective permeability of the blend. In the worst case, considering the particles to be impermeable, Maxwell's equation [17] would predict the following relationship between the steady-state permeability of the blend, P_{blend}, to that of the matrix, P_m

$$\frac{P_{\mathrm{blend}}}{P_m} = \frac{1-\phi}{1-\phi/2}, \quad (28)$$

which for ϕ = 0.1 amounts to about an 5% reduction for the blend. On the other hand, the effect of Δ on the initial flux plateau and time lag for a multilayer film can be quite significant. For time lag, it is a simple relation that incorporates the effective diffusion coefficient for the multilayer composite. If Δ = 1, the multilayer film and blend have the same time lag, otherwise, lowering Δ increases the time lag for the multilayer film, as illustrated in Fig. 15b.

The initial flux plateau, which is shown in Fig. 15a on a log scale, is extremely dependent on Δ for both blends and multilayer films, and its effect is magnified by increasing the bulk rate constant k_R. For multilayer films, decreasing Δ decreases the flux

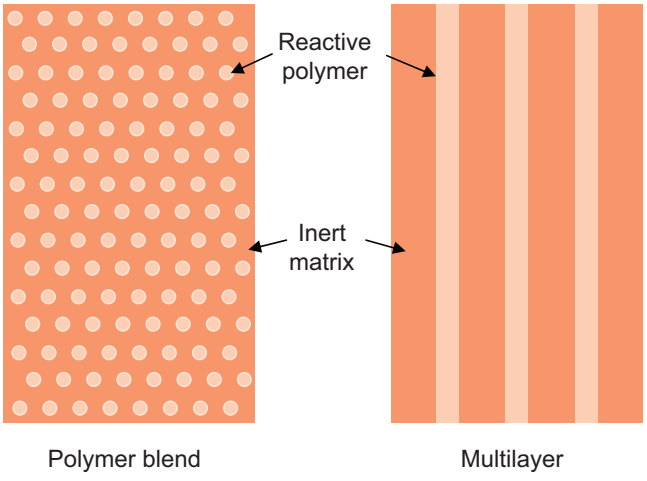

Fig. 13. Schematic illustration of a polymer blend and a multilayer barrier.

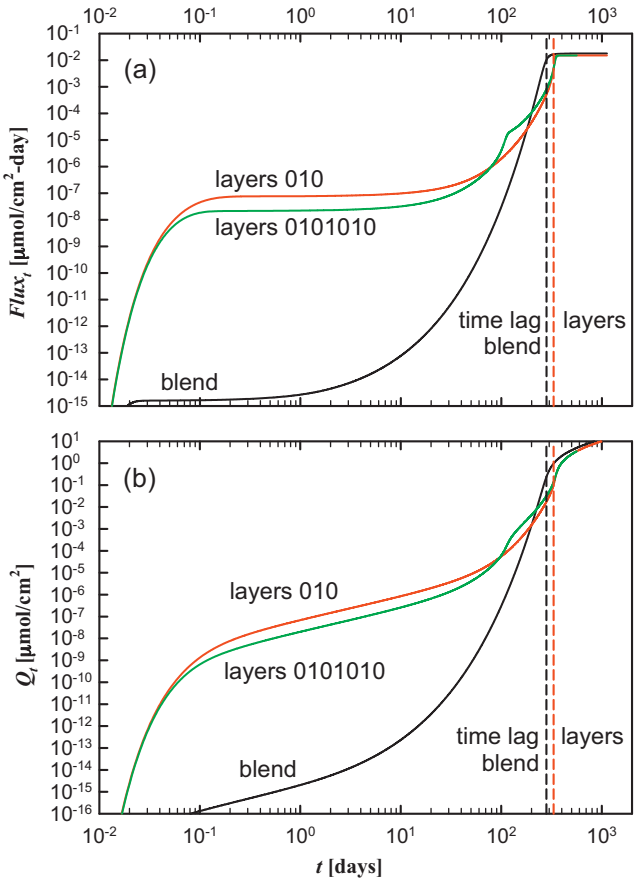

Fig. 14. (a) Downstream flux and (b) oxygen permeate versus time in log–log scale. A polymer blend is compared to multilayer films of configuration 010 and 01010, where 0 represents an inert layer, and 1 represents a reactive layer. The vertical dashed lines indicate time lag θ for each case. All parameter values are given in Table 5. Note that $\Delta = D_p/D_m = D_R/D_M = 0.357$.

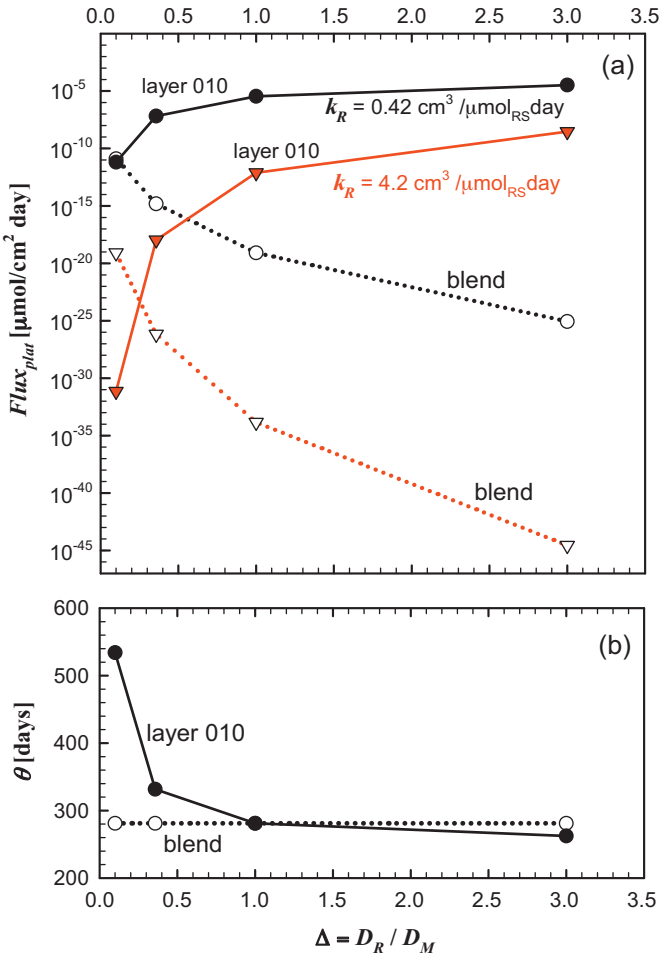

Fig. 15. Comparison of (a) downstream flux plateau in log scale and (b) time lag θ in linear scale as a function of Δ (with $D_M = 4.84 \times 10^{-4}$ cm^2/day held fixed), for a film with three layers versus a polymer blend (analytical predictions). For (a) the multilayer plateau is evaluated for two bulk reaction rates ($k_R = 0.42$ and 4.2 cm^3/μmol$_{RS}$ day, as indicated). The surface reaction rate for the blend is given by $k_p = \sqrt{k_R D_p n_{p,0}}$, to match each data point. All other parameter values are the same for the blend and multilayer films and are given in Table 5. Note that since time lag is independent of reaction rate, only one value is required for each Δ.

plateau (by orders of magnitude), while for polymer blends, the opposite is observed. The opposite effect can be explained by looking at the flux plateau equation for the blend, $J_{pl} = 2J_{SS}\Phi_b e^{-\Phi_b}$, where $\Phi_b = \sqrt{3\phi k_p L^2/D_m RH}$. When all other parameters are kept the same, decreasing $\Delta = D_p/D_m$ decreases the surface reaction, thus causing the initial flux plateau to increase. This behavior can also be explained physically: if the diffusion coefficient for the reactive particle D_p is much smaller than the diffusion coefficient for the inert matrix D_m, then there will be a greater resistance for oxygen to diffuse into the particles and reach all the reactive sites. For multilayer films, on the other hand, since the reactive and inert matrix layers are in series, slower diffusion enables oxygen to react with the immobilized sites before moving through the film. While for time lag there is a clear separation between blends and multilayer at $\Delta = 1$, consideration of the initial flux plateau requires looking at other parameters, such as the reaction rate. As illustrated in Fig. 15a, layers are favored by $\Delta \ll 1$, but higher reaction rates shift the trade point towards $\Delta = 1$.

Fig. 16 shows the effect of the partition coefficient $H = S_M/S_R$ on the downstream flux (Fig. 16a) and time lag (Fig. 16b) for two values of the bulk rate constant k_R, as in Fig. 15. Here Δ is kept constant at 0.357.

For multilayer films, varying H from 0.2 to 5 ($S_M = 4.38\ \mu\text{mol}_{O_2}/\text{cm}^3\ \text{atm}$ is held fixed) causes the initial flux plateau to increase approximately one order of magnitude, while for polymer blends the increase is of many orders of magnitude, as illustrated in Fig. 16a. The time lag for a polymer blend is independent of H while for the multilayer film, it has a linear dependence, increasing as H increases (see time lag equations in Table 4).

In summary reactive polymers with small bulk reaction rates, large diffusion and solubility coefficients (relative to the inert matrix) favor polymer blends, while reactive polymers with large bulk reaction rates and slow diffusion rates and lower solubility coefficients favor multilayer configurations. To identify the parameter values for the limiting cases where blend outperforms multilayer or vice versa, the analytical predictions summarized in Table 4 can be used, without the need to numerically solve nonlinear partial differential equations for each case.

8. Summary and conclusions

A model has been developed to describe a multilayer composite with alternating inert matrix and reactive layers. Similarly to homogeneous films and polymer blends, multilayer films initially have an initial flux plateau. However, rather than a smooth transition between this early flux plateau and the steady-state regime, intermediate inflexion points in the transient flux were observed, which coincided with the number of reactive layers in the film. Analytical predictions of the initial flux plateau and of time lag have

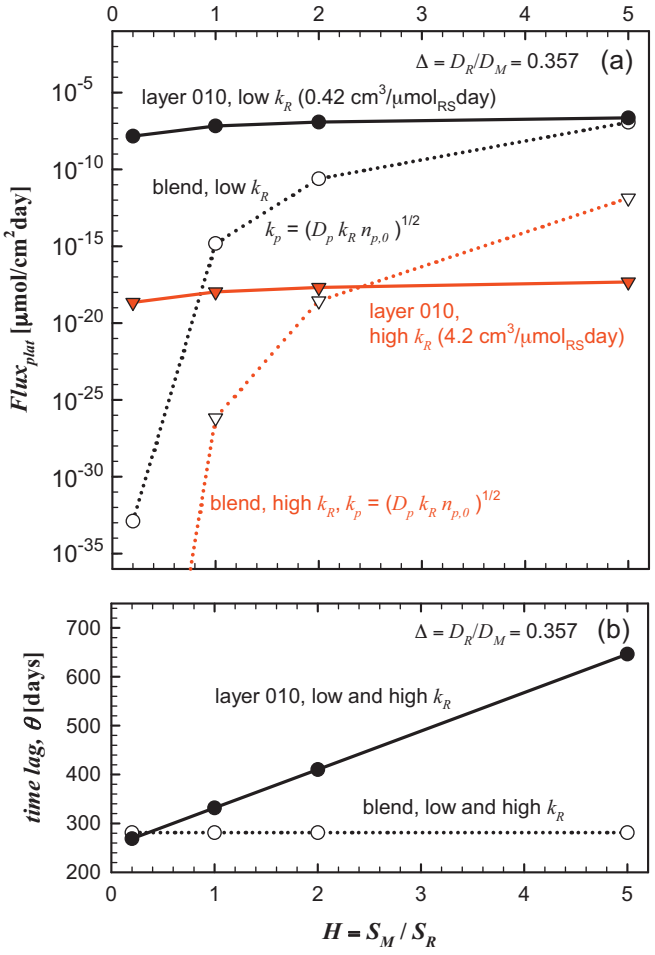

Fig. 16. Comparison of (a) downstream flux plateau in log scale and (b) time lag θ in linear scale as a function of H ($S_M = 4.38\ \mu mol_{O_2}/cm^3$ atm held fixed), for a film with three layers versus a polymer blend (analytical predictions). For (a) the multilayer plateau is evaluated for two bulk reaction rates (k_R = 0.42 and 4.2 $cm^3/\mu mol_{RS}$ day, as indicated). The surface reaction rate for the blend is given by $k_p = \sqrt{k_R D_p n_{p,0}}$, to match each data point. All other parameter values are the same for the blend and multilayer films and are given in Table 5. Note that since time lag is independent of reaction rate, only one value is required for each H.

been derived. Numerical solutions were computed for various layer configurations, to understand the changes in barrier properties do to configuration changes, such as number of layers and sequence. There are many nuances in the selection of the ideal system, as no configuration gave both the highest time lag and the lowest initial flux plateau. In general, however, systems where the first layer is inert outperform systems where the first layer is reactive. Numerical solutions were also computed for a base parameter set, and from many variations from it. In particular, ϕ, Δ and H were greatly explored.

The barrier performances of reactive polymer blends and multilayer films were compared, discussing the scenarios when it is more advantageous to use blends or multilayer films. The selection between polymer blends and multilayer films depends on the properties of both the inert matrix and the reactive polymer. When the diffusion and/or solubility coefficients of the reactive material are greater than the diffusion and/or solubility coefficients of the inert matrix, polymer blends are the most suitable choice, both in terms of time lag and initial flux plateau. On the other hand, multilayer films are more suitable for reactive materials with small diffusion and solubility coefficients relative to the matrix, particularly for higher bulk reaction rates. The analytical predictions summarized in Table 4 can be used to perform parametric studies for other parameter spaces, enabling the selection of the most suitable configuration for a particular application, obviating the need to numerically solve the partial differential equations for each case.

In these calculations it was assumed that oxidation of the reactive layers does not change the oxygen permeability of this material. We have observed experimentally that oxidation can change the permeability of these layers by a lot; it can be decreased by perhaps two orders of magnitude. This effect will make the layered systems even better barriers, and this will be addressed in future publications.

Acknowledgments

This work was supported in part by the National Science Foundation under Grant Number DMR0423914.

Nomenclature

a, b, c	coefficients in concentration equations
C	oxygen concentration in the homogeneous film, $\mu mol_{O2}/cm^3$
C_0	oxygen concentration at the film's upstream boundary, $\mu mol_{O2}/cm^3$
C_m, C_p	oxygen concentration in the polymer blend and reactive particle, respectively, $\mu mol_{O2}/cm^3$
C_M, C_R	O_2 concentration for inert matrix and reactive layers, respectively, $\mu mol_{O2}/cm^3$
D_m, D_p	oxygen diffusion coefficient of the blend inert matrix and the reactive particles, respectively, cm^2/s
D_M, D_R	oxygen diffusion coefficient for inert matrix and reactive layers, respectively, cm^2/day
H	partition coefficient, $H = S_m/S_p$ for polymer blend, $H = S_M/S_R$ for multilayer films, dimensionless
J	oxygen flux, μmol/cm^2 day
k_p	reaction rate constant for reactive particle, cm/day
k_R	reaction rate constant for reactive layers, cm^3 OSP/μmol_{RS} day
L	thickness of the film, cm
n	concentration of reactive sites, $\mu mol_{RS}/cm^3$
$n_{R,0}$	initial concentration of reactive sites in reactive layers, $\mu mol_{RS}/cm^3$
p_{O_2}	oxygen partial pressure, psia
Q_t	oxygen permeate, μmol/cm^2
R	radius of the OSP particle, cm
S_m, S_p	solubility coefficient for oxygen in the blend inert matrix and scavenging polymer particles, μmol/cm^3 atm
S_M, S_R	oxygen solubility coefficient for inert matrix and reactive layers, respectively, μmol/cm^3 atm
t	time, s
x	position in film, cm
x_F	moving front position, cm

Greek letters

β	OSP capacity, $\beta = n_0/\hat{v}$, mol_{O2}/cm^3 OSP
Δ	ratio between the oxygen diffusion coefficients for the reactive and inert matrix layers, $\Delta = D_R/D_M$, dimensionless

θ	time lag, day
θ_0	diffusion time lag of inert polymer, $\theta_0 = L^2/6D$, for homogeneous films, $\theta_0 = L^2/6D_m$ for blends, and $\theta_0 = L^2/6D_{eff}$ for multilayer films, day
ϕ	volume fraction of reactive polymer in polymer blend and in multilayer films, dimensionless
Φ_b	effective Thiele modulus for the blend, $\Phi_b = \sqrt{3\phi k_p L^2/D_m R H}$, dimensionless
Φ_H	Thiele modulus for homogeneous film, $\Phi_H = \sqrt{L^2 k_R n_0/D}$, dimensionless
Φ_p	Thiele modulus for the OSP particle, $\Phi_p = Rk_p/D_p$, dimensionless
Φ_R	Thiele modulus for reactive layers, $\Phi_R = \sqrt{(\phi L)^2 k_R n_{R,0}/D_R}$, dimensionless
ν	ratio between dissolved oxygen and reactive capacity, $\nu = \hat{\nu} C_0/n_0$ for homogeneous films, $\nu = \hat{\nu} C_{m,0}/\phi n_{p,0}$ for blends, and $\nu = \hat{\nu} S_0 p_{O_2}/\phi n_{R,0}$ for multilayer films, dimensionless
$\hat{\nu}$	stoichiometric coefficient, $\mu mol_{RS}/\mu mol_{O2}$
$\tau_{rxn,b}$	reactive time scale for polymer blend, $\tau_{rxn,b} = R/3k_p$, day
$\tau_{rxn,H}$	reactive time scale for homogeneous film, $\tau_{rxn,H} = 1/k_R n_0$, day

References

[1] M.C. Ferrari, S. Carranza, R.T. Bonnecaze, K.K. Tung, B.D. Freeman, D.R. Paul, Modeling of oxygen scavenging for improved barrier behavior: blend films, J. Membr. Sci. 329 (2009) 183–192.

[2] S. Carranza, D.R. Paul, R.T. Bonnecaze, Design formulae for reactive barrier membranes, Chem. Eng. Sci. 65 (2010) 1151–1158.

[3] S. Carranza, D.R. Paul, R.T. Bonnecaze, Analytic formulae for the design of reactive polymer blend barrier materials, J. Membr. Sci. 360 (2010) 1–8.

[4] R.G. Bauman, S.H. Maron, Oxidation of polybutadiene. I. Rate of oxidation, J. Polym. Sci. 22 (1956) 1–12.

[5] S.W. Beavan, D. Phillips, Mechanistic studies on the photo-oxidation of commercial poly(butadiene), Eur. Polym. J. 10 (1974) 593–603.

[6] V.B. Ivanov, S.G. Burkova, Y.L. Morozov, V.Y. Shlyapintokh, Kinetics of the chain-propagation and chain-termination reactions in the oxidation of polybutadiene and copolymers of butadiene with styrene, Kinet. Katal. 20/5 (1979) 1330–1333.

[7] C. Adam, J. Lacoste, J. Lemaire, Photo-oxidation of elastomeric materials. Part 1-Photo-oxidation of polybutadienes, Polym. Degrad. Stabil. 24 (1989) 185–200.

[8] M. Piton, A. Rivaton, Photooxidation of polybutadiene at long wavelengths ($\lambda > 300$ nm), Polym. Degrad. Stabil. 53 (1996) 343–359.

[9] C.D. Mueller, S. Nazarenko, T. Ebeling, T.L. Schuman, A. Hiltner, E. Baer, Novel structures by microlayer coextrusion—talc-filled PP, PC/SAN, and HDPE/LLDPE, Polym. Engr. Sci. 37/2 (1997) 355–362.

[10] D. Jarus, A. Hiltner, E. Baer, Microlayer coextrusion as a route to innovative blend structures, Polym. Engr. Sci. 41/12 (2001) 2162–2171.

[11] R.A. Siegel, E.L. Cussler, Reactive barrier membranes: some theoretical observations regarding the time lag and breakthrough curves, J. Membr. Sci. 229 (2004) 33–41.

[12] E.E. Nuxoll, R.A. Siegel, E.L. Cussler, Layered reactive barrier films, J. Membr. Sci. 25 (2005) 29–36.

[13] S.E. Solovyov, A.Y. Goldman, Optimized design of multilayer barrier films incorporating a reactive layer I. Methodology of ingress analysis, J. Appl. Polym. Sci. 100 (2006) 1940–1951.

[14] S.E. Solovyov, A.Y. Goldman, Optimized design of multilayer barrier films incorporating a reactive layer II. Solute dynamics in two-layer films, J. Appl. Polym. Sci. 100 (2006) 1952–1965.

[15] S.E. Solovyov, A.Y. Goldman, Optimized design of multilayer barrier films incorporating a reactive layer III. Case analysis and generalized multilayer solutions, J. Appl. Polym. Sci. 100 (2006) 1966–1977.

[16] J. Crank, The Mathematics of Diffusion, 2nd ed., Oxford University Press, Oxford, 1975.

[17] J.C. Maxwell, Treatise on Electricity and Magnetism, vol. I, Oxford University Press, London, 1873, p. 365.